

# Constraints on the Self-Interaction Cross-Section of Dark Matter from Numerical Simulations of the Merging Galaxy Cluster 1E 0657-56

Scott W. Randall<sup>1</sup>, Maxim Markevitch<sup>1,2</sup>, Douglas Clowe<sup>3,4</sup>, Anthony H. Gonzalez<sup>5</sup>, and Marusa Bradač<sup>6</sup>

## ABSTRACT

We compare recent results from X-ray, strong lensing, weak lensing, and optical observations with numerical simulations of the merging galaxy cluster 1E 0657-56. X-ray observations reveal a bullet-like subcluster with a prominent bow shock, which gives an estimate for the merger velocity of  $4700 \text{ km s}^{-1}$ , while lensing results show that the positions of the total mass peaks are consistent with the centroids of the collisionless galaxies (and inconsistent with the X-ray brightness peaks). Previous studies, based on older observational datasets, have placed upper limits on the self-interaction cross-section of dark matter per unit mass,  $\sigma/m$ , using simplified analytic techniques. In this work, we take advantage of new, higher-quality observational datasets by running full N-body simulations of 1E 0657-56 that include the effects of self-interacting dark matter, and comparing the results with observations. Furthermore, the recent data allow for a new independent method of constraining  $\sigma/m$ , based on the non-observation of an offset between the bullet subcluster mass peak and galaxy centroid. This new method places an upper limit (68% confidence) of  $\sigma/m < 1.25 \text{ cm}^2 \text{ g}^{-1}$ . If we make the assumption that the subcluster and the main cluster had equal mass-to-light ratios prior to the merger, we derive our most stringent constraint of  $\sigma/m < 0.7 \text{ cm}^2 \text{ g}^{-1}$ , which comes from the consistency of the subcluster's observed mass-to-light ratio with the main cluster's, and with the universal cluster

---

<sup>1</sup>Harvard-Smithsonian Center for Astrophysics, 60 Garden St., Cambridge, MA 02138, USA

<sup>2</sup>Space Research Institute, Russian Academy of Science, Profsoyuznaya 84/32, Moscow 117997, Russia

<sup>3</sup>Steward Observatory, University of Arizona, 933 N. Cherry Ave., Tuscon, AZ 85721, USA

<sup>4</sup>Department of Physics and Astronomy, Ohio University, Clippinger Lab 251B, Athens, OH 45701, USA

<sup>5</sup>Department of Astronomy, University of Florida, 211 Bryant Space Science Center, Gainesville, FL 32611, USA

<sup>6</sup>Kavli Institute for Particle Astrophysics and Cosmology, P.O. Box 20450, MS-29, Stanford, CA 94309, USA

value, ruling out the possibility of a large fraction of dark matter particles being scattered away due to collisions. Our limit is a slight improvement over the previous result from analytic estimates, and rules out most of the  $0.5 - 5 \text{ cm}^2 \text{ g}^{-1}$  range invoked to explain inconsistencies between the standard collisionless cold dark matter model and observations.

*Subject headings:* dark matter — clusters: individual (1E0657-56) — methods: numerical — large scale structure of universe

## 1. Introduction

The nature of dark matter, which accounts for the majority of the mass in the Universe, is one of the major outstanding problems of modern astrophysics. Although it is often assumed that dark matter is collisionless, there is no a priori reason to believe that this is the case, and it has been noted by other authors that a non-zero self-interaction cross-section can have important astrophysical implications (e.g., Spergel & Steinhardt 2000). In particular, self-interacting dark matter (SIDM) has been invoked to alleviate some apparent problems with the standard cold dark matter (CDM) model, such as the non-observation of cuspy mass profiles in galaxies (e.g., Moore 1994; Flores & Primack 1994; cf. Navarro et al. 1997; Moore et al. 1999b) and the overprediction of the number of small sub-halos within larger systems (e.g., Klypin et al. 1999; Moore et al. 1999a). Previous simulations and theoretical studies suggest that a self-interaction cross-section per unit mass of  $\sigma/m \sim 0.5 - 5 \text{ cm}^2 \text{ g}^{-1}$  is needed to explain the observed mass profiles of galaxies (e.g., Davé et al. 2001; Ahn & Shapiro 2003, though see also Ahn & Shapiro 2005). Earlier studies have found stringent upper limits on  $\sigma/m$ , inconsistent with the above range (e.g., Yoshida et al. 2000a; Hennawi & Ostriker 2002; Miralda-Escudé 2002, though see also Sand et al. 2002). However, in general these studies require non-trivial assumptions or statistical samples of clusters and full cosmological simulations.

Furlanetto & Loeb (2002) pointed out that if one observes an offset between the gas and dark matter in a merging cluster, arising because of the ram pressure acting on the gas but not the dark matter, it can be used to constrain the collisional nature of dark matter. Markevitch et al. (2002, hereafter M02) found just such a cluster, 1E 0657-56, which in the *Chandra* image shows a bullet-like subcluster exiting the core of the main cluster, with prominent bow shock and cold front features, and a uniquely simple merger geometry (Markevitch et al. 2002, hereafter M02). This gas bullet lags behind the subcluster galaxies, which led M02 to suggest that this cluster could be used to determine whether or not dark matter is collisional. If dark matter were collisionless, one would expect the subcluster dark matter

halo to be coincident with the collisionless subcluster galaxies. A map of the dark matter distribution was subsequently derived by Clowe et al. (2004) using weak lensing observations, which showed that the subcluster dark matter clump lay ahead of the gas bullet, close to the centroid of the subcluster galaxies (see also Clowe et al. 2006a, hereafter C06). The X-ray image of 1E 0657-56 is shown in Fig. 1 with the most recently derived weak lensing mass contours of C06 overlaid. The weak lensing contours are shown instead of the strong lensing contours since they are better for showing the overall structure, as they are derived from a wider field of view. The positions of the total mass peaks from strong and weak lensing analyses are consistent with one another, and the general structures are similar. The more massive main cluster is on the left and the high-velocity merging bullet subcluster is on the right. The main and subcluster mass peaks are clearly visible in the mass map, as is the offset between the gas bullet and the corresponding dark matter (DM) peak. C06 argued that this offset is direct evidence for the existence of dark matter.

The weak lensing mass map of Clowe et al. (2004) was used by Markevitch et al. (2004, hereafter M04), in conjunction with the X-ray and optical observations available at the time, to analytically estimate upper limits on the self-interaction cross-section per unit mass of DM,  $\sigma/m$ , using three independent methods. These methods were based on the observed offset between the gas bullet and the DM subclump, the high merger velocity of the subcluster, and the survival of the DM subclump (more precisely, the subcluster’s  $M/L$  ratio being equal to that observed in other clusters and in the main cluster). M04 assume a King mass profile, based on the original weak lensing mass map, and that the subcluster has passed only once through the main cluster, close to the main cluster core, as indicated by the X-ray image. Their most stringent limit comes from the observed survival of the DM subclump, from which they infer that  $\sigma/m < 1 \text{ cm}^2 \text{ g}^{-1}$ .

Although the analytic estimates performed by M04 provide useful upper limits on  $\sigma/m$ , several conservative simplifying assumptions were necessary. For instance, the effects of dynamical friction as the subcluster disturbs the main cluster mass distribution were ignored, as was the possibility of multiple scatterings per particle. Although these effects are relatively small, their inclusion may lead to tighter constraints. Furthermore, the analytic estimates cannot address any structure that may be found in a high-resolution mass map (e.g., tails in the DM distribution, similar to the gas tails seen in the bullet, due to collisional stripping of DM, as described by M04). This argues for full N-body simulations that would include the effects of SIDM with varying cross-sections.

Additionally, new data (both X-ray and lensing) have become available for 1E 0657-56. Analysis of data from 450 ks of total exposure with *Chandra* gives a more accurate shock Mach number of  $M = 3.0 \pm 0.4$  (all uncertainties 68%), which corresponds to a shock (and

bullet) velocity of  $4700 \pm 630$  km s $^{-1}$  (Markevitch 2005). Recent weak and strong lensing analyses of a much larger optical dataset, which includes *HST* observations, give a higher quality mass map and a more accurate determination of the subcluster dark matter and galaxy centroids (Bradač et al. 2006, hereafter B06; C06). In particular, the accuracy of the total mass and galaxy centroids is now sufficient for an additional method of constraining  $\sigma/m$ . In this paper, we will concentrate on the most sensitive method from M04, which is based on the observed mass-to-light ( $M/L$ ) ratios, and on this new test. The best way to interpret the new high-quality data is through comparisons with detailed numerical simulations of the merger which allow for SIDM with varying cross-sections. We present results from such simulations and give constraints on the self-interaction cross-section of dark matter particles. We assume  $\Omega_0 = 0.3$ ,  $\Omega_\Lambda = 0.7$ , and  $H_0 = 70$  km s $^{-1}$  Mpc $^{-1}$ , for which  $1'' = 4.42$  kpc at the cluster redshift of  $z = 0.296$ .

## 2. The Simulations

### 2.1. Simulation Code and Parameters

All simulations were performed using a modified version of the publicly available TreeSPH code GADGET2 (Springel 2005). To model the self-interaction of the DM particles, we adopted a Monte Carlo method used previously by other authors (e.g., Burkert 2000; Yoshida et al. 2000b). At each simulation time step, the scattering probability for the  $i$ th particle is given by

$$P_i = \rho_i \sigma v_{\text{rel}} \Delta t, \quad (1)$$

where  $\rho_i$  is the local density,  $v_{\text{rel}}$  is the relative velocity between the  $i$ th particle and its nearest neighbor, and  $\Delta t$  is the time step size. The local density is determined using GADGET2’s smoothed particle hydrodynamic (SPH) capabilities. Collisions are assumed to be elastic and scattering isotropic in the center-of-mass frame. In order for this relation to be valid,  $\Delta t$  must be chosen such that  $P_i \ll 1$ .

We ran a series of merger simulations with  $\sigma/m$  varying between 0 and  $1.25$  cm $^2$  g $^{-1}$ . Each simulation run included  $10^6$  DM particles (gas was not included in the simulations, see discussion in § 4.5). Additionally, we performed a convergence test run with  $10^7$  DM particles and  $\sigma/m \approx 1$  cm $^2$  g $^{-1}$ , which agreed well with the lower resolution run for all tests we performed. We interpret this agreement as indicating that the effects of individual self-interacting DM particles are well modeled by the large computation particles used in the simulations, and that the results we present here are not seriously affected by numerical resolution effects. The ratio of DM particles in the main cluster and subcluster was set equal

to the initial total mass ratio of the clusters, which is known analytically from the King models used to build the clusters.

In this work, we apply a new method for constraining  $\sigma/m$  based on the absence of an offset between the subcluster total mass and galaxy centroids. For this, we added another family of particles to the simulations to represent the collisionless galaxies. We choose  $10^5$  “normal” galaxy particles for the main cluster and  $2.5 \times 10^4$  for the subcluster throughout. The ratio of the number of normal galaxy particles was estimated based on galaxy counts given by Barrena et al. (2002). The galaxies were initially distributed like the DM in each run. The mass in galaxies was assumed to be roughly 5% of the total mass for each cluster, which, combined with the number of galaxy particles, gives a low mass per galaxy ( $2.15 \times 10^8 M_\odot$ ). Using a large number of light-weight galaxies was chosen over using a more realistic mass per galaxy so that accurate galaxy centroids could be determined. Test simulations run with the more realistic average mass per galaxy of  $10^{11} M_\odot$ , also determined from results given by Barrena et al. (2002), showed similar results to those given below in §3, though, as expected, with a larger scatter. Two cD galaxies, one at the center of each cluster, were also included in the simulations (though we note that three cD galaxies are observed, two associated with the main cluster and one with the subcluster). Their inclusion leads to conservative estimates of the effects of DM self-interaction, since a lower central DM density is required to reproduce the observed total mass profile (and the scattering probability depends on the local DM density via Eqn. 1). The cD galaxies were each given a mass of  $10^{13} M_\odot$ .

The gravitational softening length was chosen to be 2 kpc throughout, which is on the order of the mean inter-particle separation in the densest region in each simulation (i.e., at core passage). The softening length for the cD galaxy particles was set to 60 kpc throughout. This large softening length was chosen since on the scale of the simulations cD galaxies are significantly extended objects and treating them as concentrated point-like masses would be unrealistic. Since the lensing observations do not give an accurate mass profile for the subcluster, King models with density profiles of  $\rho(r) = \rho_0(1 + r^2/r_c^2)^{-3/2}$ , where  $\rho_0$  is the central density and  $r_c$  is the core radius, were conservatively chosen for the mass profiles of each cluster. Such a choice gives conservative limits for the effects of self-interacting DM, since King models do not have strongly concentrated “cuspy” cores, as compared to NFW (Navarro et al. 1995) and Hernquist (1990) profiles. Thus the central density is lower and the total number of DM particle collisions is conservatively reduced. Further discussion of the impact of the bullet mass profile on our results can be found in §4.2. As suggested by the X-ray morphology (M04), all simulated mergers were head-on collisions with zero impact parameter and an initial separation of 4 Mpc. The effects of a possible non-zero impact parameter are discussed in §4.1.

## 2.2. Initial Conditions

For each run, the initial conditions were chosen such that the projected mass profiles of the main cluster and the bullet subcluster, after core passage and at the observed separation (720 kpc), roughly matched those from the most recent combined strong and weak lensing results derived by B06, which are given in the last row of Table 2. A relatively small contribution from the observed distribution of gas mass was subtracted from the B06 total mass, so that the resulting values could be directly compared with the simulations. The gas masses were computed from the X-ray observations. The details of the derivation of the gas mass map will be given in a future paper. A summary of the parameters for each simulation run is given in Table 1, which gives the initial central density and core radius for the main cluster ( $\rho_{c,1}$ ,  $r_{c,1}$ ) and the bullet subcluster ( $\rho_{c,2}$ ,  $r_{c,2}$ ), and  $\sigma/m$  for each run. The mass profiles were truncated at 20  $r_c$ .

As pointed out by C06, weak lensing is expected to underestimate the mass of the lens by 10-20% in the dense central regions. Furthermore, weak lensing can underestimate masses due to mass-sheet degeneracy, where the mass map is affected by the non-detection of mass at the edges of the field of view. The effect can be seen by comparing the total (i.e., without the gas mass subtracted) weak lensing mass estimates of C06 to the mass profiles derived by B06, which combine strong and weak lensing observations. We chose to match the projected mass profiles in the simulations to those given by B06, since strong lensing is expected to give better results in the central core regions. We are most interested in these regions since most of the particle scattering depth accumulates near the center. We explore the effects of decreasing the total mass of the system on our results in § 4.3.

## 2.3. Matching Simulations to Observations

Columns 4 & 5 of Table 2 give the total projected mass within 150 kpc of the mass peak for the main cluster ( $M_1(r < 150\text{kpc})$ ) and the subcluster ( $M_2(r < 150\text{kpc})$ ) at the observed separation for each simulation run and from the lensing observations. Some trial-and-error was necessary to determine what initial conditions gave the desired projected mass profiles at the desired separation. In general, larger  $\sigma/m$  values required a more concentrated subcluster initially. This effect occurs because the self-interaction of the DM particles causes them to be scattered away, particularly in high density regions. Consequently, the subcluster mass profile is spread out during core passage. For the purposes of comparing the simulations with observations, we take the simulation snapshot where the offset between the clusters is closest to the observed separation. The time resolution of the snapshots was small enough to match this value to within a few kpc ( $< 1''$ ), which is within the observational error. We

require the simulated mass profiles at this moment to be consistent with the strong lensing mass map to within 10% in the inner regions ( $r < 500$  kpc).

## 2.4. Stability of Simulated Halos

It is of interest to evaluate the stability of our simulated clusters, particularly in the presence of SIDM. In the case of non-self-interacting DM, the phase-space distribution function can be computed and used to generate a gravitationally stable King model density profile. However, in the case of SIDM, particle collisions will tend to transfer kinetic energy from one region of the cluster to another, consequently altering the density profile (see, e.g., Burkert 2000). In section § 3.2, we will draw conclusions based on the fraction of particles scattered away from the core of the subcluster due to the merger event. It is therefore necessary to determine what fraction of particles might flow from the central region of the bullet due to the instability resulting from SIDM collisions. To this end, we ran simulations of the subcluster DM halo, allowing it to evolve in isolation over the timescale of the merger simulations (about 1 Gyr). We used the same cluster parameters as the subcluster that has the highest central density of all the clusters in Table 1. The results are shown in Figure 3, which gives the initial density profile (solid line) and the density profile after 1 Gyr for  $\sigma/m = 0$  cm<sup>2</sup> g<sup>-1</sup> (dotted line) and  $\sigma/m = 0.7$  cm<sup>2</sup> g<sup>-1</sup> (dashed line). The density in the inner regions is marginally enhanced in the case of SIDM. This result is similar to the core-collapse phase seen by Burkert (2000), where weak interactions between the kinematically hot core and the cooler outer regions result in an outward transport of kinetic energy (though this effect is expected to be somewhat curtailed here due to the near isothermality of the King profile at small radii). For the purposes of the test described in § 3.2, we are only concerned with the total mass within *projected* radii. This quantity is plotted for each run in Figure 4. The above effect of SIDM on the projected mass profile is negligible, particularly for projected radii  $x \geq 150$  kpc, which is the minimum radius considered for the test described in § 3.2. Thus, if we find that a large fraction of SIDM particles scattered outside this radius, it can be assumed to be caused by the merger event as opposed to any halo instability. Furthermore, the collisionless galaxies are expected to adjust to any change in the overall potential (which is dominated by the DM), thereby acting to further stabilize the mass-to-light ratio. Indeed, in these isolated subcluster runs, the mass-to-light ratios within a projected radius of 150 kpc from the cluster centers stay within 2% of their initial values, regardless of the DM self-interaction.

### 3. Results

#### 3.1. Galaxy – Dark Matter Centroid Offset

For non-self-interacting DM, the centroids of the subclump DM and galaxy distributions are expected to be coincident throughout the simulation, since gravity is the only operating force. However, when  $\sigma/m > 0$ , the subcluster DM halo experiences a drag force as it passes through the main cluster, and subsequently lags the collisionless galaxies, just as the fluid-like subcluster gas core is observed to lag the DM halo (see Fig. 1). We ran simulations with a range of values for  $\sigma/m$  and calculated the centroids for each particle type by taking the average projected position of the particles in some large region, centering on this position with a smaller region, and repeating with smaller and smaller regions (down to a region with a radius of 200 kpc). Column 6 of Table 2 gives  $\Delta x$ , the offset between the subcluster galaxy and DM centroids, for each run, for the moment when the subcluster is close to the observed separation of 720 kpc from the main cluster. The dependence of  $\Delta x$  on  $\sigma/m$  is also plotted in Figure 5 (solid line). Results from the run with  $\sigma/m = 0$  indicate that the offsets from the simulations are accurate to about  $\pm 2$  kpc ( $0.5''$ ). It is clear from Table 2 that the centroid offset is a strong function of  $\sigma/m$ .

An X-ray image close-up of the bullet region with error contours for the subcluster total mass and galaxy centroids overlain is shown in Figure 2. Details of the derivation of the total mass centroids are given in C06. The centroid of the galaxy distribution was calculated from the ACS photometry, using all galaxies for which the F814W-F606W color is within 0.15 mag of the red sequence. We used an Epanechnikov kernel with  $h = 30''$  (Merritt & Tremblay, 1994; Gonzalez et al. 2002) to determine the centroid, and a bootstrap technique to quantify the uncertainty. The centroid of the subcluster galaxies is found to be  $5.7'' \pm 6.6''$  ( $25 \pm 29$  kpc) west of the corresponding weak lensing mass peak. Given the observational errors on the centroid positions (roughly  $5''$ , or 22 kpc, on the subcluster mass peak and galaxy centroid), the absence of a larger offset means that  $\sigma/m < 1.25 \text{ cm}^2 \text{ g}^{-1}$ . We note that, although this upper limit is greater than the best constraint of  $\sigma/m < 1 \text{ cm}^2 \text{ g}^{-1}$  found by M04, it is more robust, since it does not rely on the assumption that the subcluster and the main cluster had equal  $M/L$  ratios prior to the merger, as is the case with the limit from M04 (see § 3.2). This distinction is relevant since, although there is evidence for a universal  $M/L$  ratio for clusters, the level scatter for individual clusters is not negligible (see Dahle 2000).

### 3.2. Subcluster M/L Ratio

In a merger scenario, SIDM is expected to give a lower  $M/L$  ratio for the subcluster that has just passed through a dense core as compared to collisionless DM. This is because during the merger, DM particles are scattered away due to collisions, while the collisionless galaxies are relatively unaffected. To estimate the change in the  $M/L$  ratio in the simulations due to the merger, we simply take the ratio of the total mass to galaxy mass within 150 kpc (projected) of the bullet DM centroid and compare the values at the start of the simulations and at the observed separation. The results are tabulated in Column 7 of Table 2, which gives  $f$ , the fractional decrease in the bullet  $M/L$  ratio within 150 kpc, and also plotted in Figure 5 (dashed line). We note that for  $\sigma/m \approx 1 \text{ cm}^2 \text{ g}^{-1}$ , the subcluster loses about 38% of its mass within 150 kpc, which is in agreement with a conservative estimate of 20 - 30% given by M04. As expected, the numerical results yield somewhat tighter constraints on  $\sigma/m$  as compared to the analytic estimates when using the same method and observational constraints.

Using the latest lensing mass map from B06, we rederived  $M/L$  ratios for each of the two subcluster within a projected 150 kpc of the total mass peaks (for previous results see Clowe et al., 2004). For the subcluster, the mass contribution from the outskirts of the main cluster has been approximately subtracted, whereas for the main cluster, the total mass is used, since the contribution from the subcluster is negligible. The projected mass contribution from the main cluster to the subcluster is estimated by taking the average mass in an annulus at the distance of the subcluster (excluding the region of the subcluster itself). This gives a conservative estimate for the upper limit on  $\sigma/m$ , since scattering due to putative DM collisions is expected to result in an anomalously low  $M/L$  value for the subcluster as compared to the main cluster, and by reducing the observed mass of the subcluster we minimize the effect of the collisions that we want to constrain. We find  $M/L_B = 471 \pm 28, 422 \pm 25$  and  $M/L_I = 179 \pm 11, 214 \pm 13$  for the subcluster and the main cluster, respectively (for a discussion of the errors on the mass measurements, see B06). The ratios agree with one another to within about the 68% confidence intervals. From the  $I$  band data, we find that the ratio of  $M/L$  ratios of the subcluster and main cluster is  $0.84 \pm 0.07$ . We conservatively choose to use the  $I$  band data only, since we want to put a firm lower limit on this ratio, and  $M/L_B$  is larger for the subcluster than for the main cluster. Assuming each cluster started out with similar  $M/L$  values, which appears to be a reasonable assumption for clusters in general (e.g., Mellier 1999; Dahle 2000), we conclude that the subcluster could not have lost more than  $\sim 23\%$  of its initial mass. A comparison with the results from simulations plotted in Figure 5 (dashed line) shows that this implies  $\sigma/m \lesssim 0.6 \text{ cm}^2 \text{ g}^{-1}$ , which is a slight improvement over the previous best limit of  $\sigma/m \lesssim 1 \text{ cm}^2 \text{ g}^{-1}$  from the conservative estimates of M04.

### 3.3. Structure in Subcluster Dark Matter Distribution

M04 suggested that scattered DM particles, which would account for about 1/5 of the total subcluster mass, might form tail features in the DM distribution, similar to the tails seen in the X-ray image of the gas bullet (see Figure 1). The simulations allow us to determine whether the non-observation of such tails in the mass map could be used to constrain  $\sigma/m$ . We find that, rather than forming a tail, the scattered particles are mostly deposited in the core of the main cluster, and do not form any features at a level that is interesting for constraining  $\sigma/m$ .

## 4. Discussion

### 4.1. Non-zero Impact Parameter

As M04 argue, the morphology of the X-ray image, in particular, the symmetry of the North-South X-ray bar (most likely an oblate spheroid viewed edge-on) between the main cluster and subcluster mass peaks around the axis of symmetry set by the shape of the X-ray bullet (which gives its present velocity direction), combined with the line-of-sight velocity and X-ray derived Mach number, indicate a merger axis that is  $\sim 10^\circ$  from the plane of the sky, and that the cluster cores must have passed close to one another, certainly within the  $\sim 200$  kpc core radius of the main cluster. In all simulations previously discussed, it was assumed that the bullet subcluster passed directly through the center of the main cluster core, i.e., that the impact parameter of the merger,  $b$ , is zero. For  $b > 0$ , we expect that the effects of self-interacting DM will be reduced, since the density is at a maximum when the core centers pass directly through one another, and the scattering probability is proportional to the density (Eqn. 1). To test the strength of this effect, we re-ran the simulation R4 (see Table 1) with an impact parameter of  $b = 200$  kpc. Aside from the impact parameter, the initial mass and velocity distributions were identical to those for run R4, so that the relative effects of  $b > 0$  could be investigated (specifically, no adjustments were made to the initial conditions to more closely match the current observed mass profiles). The resulting projected total mass profiles for the subcluster within 150 kpc and 250 kpc at the observed separation agreed with those from the  $b = 0$  run to within 4%. For the main cluster, the match was better than 1%.

The resulting offset between the galaxy and DM centroids during the post core passage phase was systematically smaller than the offset seen in the  $b = 0$  run. At the observed separation, the difference in the centroid offsets, as compared to the  $b = 0$  run, was about 4 kpc, which is on the order of both the observational error and the accuracy of our numerical

technique. The fractional change in the  $M/L$  ratio of the subcluster was similarly affected; for the  $b = 0$  case, the  $M/L$  ratio within 150 kpc drops by about 27%, whereas for the run with  $b = 200$  kpc, it drops by 22%. Assuming, as we did in § 3.2, that the subcluster could not have lost more than  $\sim 23\%$  of its initial mass, we find the constraint that  $\sigma/m < 0.7 \text{ cm}^2 \text{ g}^{-1}$ . We therefore conclude that, although a non-zero impact parameter reduces the effects of self-interacting DM as expected, the level of the effect is relatively small. This is likely due to the assumed King mass profile of the main cluster. The radial density gradient is relatively small within the core radius of the main cluster (which in this case is 151 kpc), so it is not surprising that the effects of self-interacting DM are not significantly reduced by increasing the impact parameter, so long as it is comparable to the core radius of the main cluster. Naturally, the effects of a non-zero  $b$  would be increased if the main cluster had a strongly peaked mass profile, though the current lensing data suggest otherwise. We conclude that any value of impact parameter that is consistent with the observations will only slightly alter our results.

## 4.2. Alternative Bullet Mass Profiles

As noted in §2, the choice of a King mass profile for the subcluster is expected to give conservative estimates on the effects of collisional DM, based on the  $M/L$  ratio, since the central density is low as compared to models with cuspy cores such as NFW and Hernquist models. However, in the case of the galaxy/DM centroid offset test, one might argue that since the subcluster galaxies are more tightly bound in the center for more highly concentrated mass profiles, it will be more difficult to displace them, which could lead to a smaller offset between the centroids despite the increased action of DM collisions. We therefore ran a test simulation, using a King model for the main cluster and a Hernquist model for the subcluster, with  $\sigma/m = 0.72 \text{ cm}^2 \text{ g}^{-1}$ . The Hernquist profile is given by

$$\rho(r) = \frac{Ma}{2\pi r} \frac{1}{(r+a)^3}, \quad (2)$$

where  $M$  is the total cluster mass and  $a$  is the scale length (Hernquist 1990). As before, initial parameters were chosen such that the bullet mass profile roughly matches the observed profile at the current separation (we used  $M = 3.13 \times 10^{14} \text{ M}_\odot$ ,  $a = 100$  kpc). This is expected to be the most conservative model combination for this test, since the main cluster King model minimizes the effects of DM self-interaction while the subcluster Hernquist model maximizes the binding energy of the subcluster galaxies. The results show that, when comparing to run R4 in Table 2, the galaxy/DM centroid offset was only slightly less than that found with the King model subcluster, on the order of the accuracy of the simulation offset values (less than

1 kpc). The change in the subcluster’s  $M/L$  was similarly only weakly affected ( $f = 0.27$  for the King model bullet subcluster, whereas for the Hernquist model we find  $f = 0.31$ , consistent with the King profile being the conservative case). The agreement is likely due to the fact that the centroids become offset from one another after core passage, and it is during core passage that the central density peak of the bullet is mostly “smoothed away” due to DM collisions (recall that DM scattering is more frequent in high density regions, so high density structures are more efficiently destroyed by DM self-interactions). Although strongly peaked density profiles have been found to be unstable to SIDM (e.g., Burkert 2000; Yoshida et al. 2000b), in our simulation a significant change in density only occurred at small radii, such that the total projected mass of the subcluster within 50 kpc remained stable up until the merger event. Therefore the subcluster mass distribution remained significantly more peaked than a King profile cluster with the same projected mass within 150 kpc. We conclude that our results are only weakly dependent on the mass profile chosen for the bullet, so long as we require that the observed mass profile is reproduced. For the initially more centrally concentrated profiles, the effects of the increased binding energy in the core are balanced by the increased scattering frequency in this region.

### 4.3. Mass Profile Dependence

As mentioned in § 2, weak lensing is expected to underestimate the mass of the lens by 10-20%. There are two separate effects that contribute to this underestimation. First, near the core of a cluster there is a large region without weak lensing galaxies, and this region is effectively smoothed over when computing the mass map. Additionally, galaxies near the regions where strong lensing dominates are measured in the weak lensing approximation, which also leads to an underestimate of the mass in the core. Second, the total cluster mass can be underestimated due to mass-sheet degeneracy, where the mass-map is affected by the non-detection of mass at the edge of the field of view. Although projection of foreground and/or background structures unassociated with the clusters will artificially increase the mass, it is highly unlikely that such projected structures significantly contributed to the detected lensing signal (C06). Results from strong lensing, which is not susceptible to the same systematic underestimation as weak lensing, do indeed give systematically higher projected masses for this system, by about a factor of 2 within the inner few hundred kpc, which is the region we are most interested in for this analysis (compare B06 and C06; see C06 for further discussion of this discrepancy). Though we chose to use the mass estimates from strong lensing, since it should give a more reliable estimate of the projected mass near the cluster cores, it is interesting to explore the dependence of our results on the lensing mass estimates. To this end, we conducted a simulation run similar to run R4, but with the initial cluster

central densities chosen such that the projected mass profiles at the observed separation were about 2 times lower than the masses derived from strong lensing observations, roughly in agreement with the weak lensing results given by C06 (the initial core radii were the same as for run R4). Since the scattering probability depends on the density, we expect these less massive halos to be more weakly affected by SIDM.

Results obtained from the simulations with the lower mass normalization show that the effects of SIDM are diminished, as expected for a linear dependence of the scattering probabilities on the projected mass. In run R4, the  $M/L$  ratio dropped by 27%, whereas for the run with 1/2 the total mass it dropped by 14% (roughly a factor of 2 less). Similarly, the galaxy/DM centroid offset was 11.1 kpc, again, about a factor of 2 down from the 24.1 kpc offset seen in run R4. If we assume that this factor of two effect can be applied to all of values given in columns 6 & 7 of Table 2 and consider the more sensitive  $M/L$  test, we find that requiring  $f \lesssim 0.20$  would correspond to  $\sigma \lesssim 1.25 \text{ cm}^2 \text{ g}^{-1}$ . This is done as a test of the method only, since these low halo mass values are not realistic, as they are insufficient to produce the system of strong arcs observed in the *HST* images (C06).

#### 4.4. Low Merger Velocity

All of the simulations discussed so far have assumed a merger velocity that is consistent with that derived from X-ray observations (Markevitch, 2005), which give a Mach number for the shock front of  $M = 3.0 \pm 0.4$ , and it is assumed that the subcluster has the same velocity as the shock (though see Springel & Farrar, 2007). Since the subcluster could have slowed down, or the shock front accelerated, it is interesting to ask what effect a lower velocity would have on the inferred upper limit on  $\sigma/m$ , particularly since the observed velocity is larger than would be expected from free fall of the subcluster onto the main cluster (Farrar & Rosen 2007). In order to test the dependence of our upper limit on merger velocity, we ran a simulation with  $\sigma/m = 0.72 \text{ cm}^2 \text{ g}^{-1}$  such that the relative velocity of the cluster DM halos at observed separation was 1.5 times lower, about  $3100 \text{ km s}^{-1}$  ( $M \approx 2$ ). This is close to the expected free-fall velocity of the subcluster, and to the relative velocity of  $2860 \text{ km s}^{-1}$  found by Springel & Farrar (2007) from hydrodynamical simulations of this system. The results showed little difference from the higher velocity run (compare to run R4 in Table 2):  $\Delta x$  was 30.2 kpc (vs. 24.1 kpc) and  $f$  was 0.25 (vs. 0.27). We therefore conclude that our results are relatively insensitive to merger velocities that are not in large disagreement with the observations. A weak dependence of the  $M/L$  ratio on the subcluster velocity  $v$  is easy to understand: the particle scatters out of the subcluster as long as  $v/2$  is much greater than the escape velocity from the subcluster, which it is by a large margin (M04).

#### 4.5. Effects of Diffuse Gas

As mentioned in § 2, the intracluster gas observed in the X-ray band was not included in the simulations (doing so would greatly increase the computing time and the complexity involved with matching the observations in detail). The only way for the gas to affect the results is via gravitational interaction (we ignore the possibility of non-gravitational baryon-DM interactions, the cross-section of which has been shown to be extremely small, e.g., Chen et al. 2002). In general, the gas is expected to contribute about 10% of the total mass of the system, a figure which appears to be consistent with the lensing and X-ray observations (B06). One might worry that, when matching the observed mass profiles, some “extra” DM is needed to account for the missing gas. As mentioned in § 2, gas masses have been subtracted from the lensing masses using a detailed model of the gas distribution derived from fitting the X-ray observations. In terms of the test involving the decrease in the subcluster  $M/L$  ratio (see § 3.2), we needn’t worry about the subcluster gas for the simple reason that the gas bullet is far from the subcluster mass peak (roughly 23'', or 102 kpc). Therefore, the gas in the region of the bullet mass peak is not centrally concentrated and will not significantly add to the binding energy of potentially scattered DM particles. For the galaxy and total mass centroid offset test (see § 3.1), the exclusion of the gas is expected to give a conservative result: the gas bullet and bar feature seen in Figure 1 will act to decelerate the subcluster DM halo and galaxies. However, if, as is the case with SIDM, the DM halo starts to lag behind the galaxies and gets closer to the gas cores than the main concentration of the galaxies, it will experience a larger deceleration, thereby increasing the offset between the two. Due to the relatively low mass of the gas components, and the large distance between the gas peaks and the subcluster DM halo and galaxies (as compared to the offset of the latter), the strength of this effect will be quite small. We therefore conclude that including gas in the simulations would not significantly affect our results.

### 5. Summary

We have combined results from new X-ray, optical and lensing observations and our N-body simulations of the merging galaxy cluster 1E 0657-56 in order to derive an upper limit on the self-interaction cross-section of dark matter particles,  $\sigma/m$ . We give constraints on  $\sigma/m$  based on two independent methods: from the lack of offset between the total mass peak and galaxy centroid of the subcluster that would arise during the merger due to drag on the subcluster halo from DM particle collisions, and from the lack of a decreased mass-to-light ratio of the subcluster due to scattering of DM particles. From the former, we find  $\sigma/m < 1.25 \text{ cm}^2 \text{ g}^{-1}$ , and from the latter,  $\sigma/m < 0.7 \text{ cm}^2 \text{ g}^{-1}$ , which includes the

uncertainty in the impact parameter of the merger (upper limits are from 68% confidence intervals). Our best constraint is a modest improvement of the previous best constraint from conservative analytic estimates of  $\sigma/m < 1 \text{ cm}^2 \text{ g}^{-1}$  (M04). Furthermore, our limit of  $\sigma/m < 1.25 \text{ cm}^2 \text{ g}^{-1}$  is more robust than the best analytic limit, since this method does not depend on the assumption that the subcluster and main cluster  $M/L$  ratios were equal prior to the merger. Previous studies have found that  $\sigma/m \sim 0.5-5 \text{ cm}^2 \text{ g}^{-1}$  is needed to produce the observational effects that self-interacting dark matter has been invoked to explain (e.g., non-peaked galaxy mass profiles and the underabundance of small halos within larger systems). Our results rule out almost this full range of values, at least under the assumption that  $\sigma$  is velocity-independent.

We would like to thank Volker Springel, Naoki Yoshida, Yago Ascasibar, and Alexey Vikhlinin for useful discussions and for providing access to various private codes. Simulations were performed on a Beowulf cluster at the ITC in the Harvard-Smithsonian Center for Astrophysics. Support for this work was partially provided for by the NASA *Chandra* grants G04-5152X and TM6-7010X, and NASA contract NAS8-39073.

## REFERENCES

Ahn, K., & Shapiro, P.R. 2003, J. Korean Astronomical Soc., 36, 89  
Ahn, K., & Shapiro, P.R. 2005, MNRAS, 363, 1092  
Barrena, R., Biviano, A., Ramella, M., Falco, E. E., & Seitz, S. 2002, A&A, 386, 816  
Bradač, M., Clowe, D., Gonzalez, A. H., Marshall, P., Forman, W., Jones, C., Markevitch, M., Randall, S., Schrabback, T., & Zaritsky, D. 2006, ApJ, 652, 937 (B06)  
Burkert, A. 2000, ApJ, 534, L143  
Chen, X., Hannestad, S., & Scherrer, R. J. 2002, Phys. Rev. D65, 123515  
Clowe, D., Gonzalez, A. H., & Markevitch M. 2004, ApJ, 604, 596  
Clowe, D., Bradač, M., Gonzalez, A. H., Markevitch, M., Randall, S. W., Jones, C., & Zaritsky, D. 2006a, ApJ, 648, L109 (C06)  
Clowe, D., Randall, S. W., Markevitch, M. 2006, Proceedings of the 2006b UCLA Dark Matter Symposium (astro-ph/0611496)  
Dahle, H. 2000, Proceedings of The NOT in the 2000's, Eds. N. Bergvall, L. O. Takalo, & V. Piironen (Univ. of Turku), 45  
Davé, R., Spergel, D. N., Steinhardt, P. J., & Wandelt, B. D. 2001, ApJ, 547, 574

Farrar, G. R., Rosen, R. A. 2007, in 2007 AAS/AAPT Joint Meeting, American Astronomical Society Meeting 209, #37.04.AAS, 370

Flores, R. A., & Primack, J. R. 1994, *ApJ*, 427, L1

Furlanetto, S. R., & Loeb, A. 2002, *ApJ*, 565, 854

Gonzalez, A. H., Zaritsky, D., Simard, L., Clowe, D., White, S. D. M. 2002, *ApJ*, 579, 577

Hennawi, J. F., & Ostriker, J. P. 2002, *ApJ*, 572, 41

Hernquist, L. 1990, *ApJ*, 356, 359

Klypin, A., Kravtsov, A. V., Valenzuela, O., & Prada, F. 1999, *ApJ*, 522, 82

Merritt, D., Tremblay, B. 1994, *AJ*, 108, 514

Miralda-Escudé, J. 2002, *ApJ*, 564, 60

Navarro, J. S., Frenk, C. S., & White, S. D. M. 1995, *MNRAS*, 275, 720

Navarro, J. S., Frenk, C. S., & White, S. D. M. 1997, *ApJ*, 490, 493

Markevitch, M., Gonzales, A. H., David, L., Vikhlinin, A., Murray, S., Forman, W., Jones, C., & Tucker, W. 2002, *ApJ*, 567, L27 (M02)

Markevitch, M., Gonzales, A. H., Clowe, D., Vikhlinin, A., Forman, W., Jones, C., Murray, S., Tucker, W. *ApJ*, 606, 819 (M04)

Markevitch, M. 2005, in Proceedings of The X-ray Universe 2005, San Lorenzo de El Escorial, Spain (in press, astro-ph/0511345)

Mellier, Y. 1999, *ARA&A*, 37, 127

Moore, B. 1994, *Nature*, 370, 629

Moore, B., Ghigna, S., Governato, F., Lake, G., Quinn, T., Stadel, J., & Tozzi, P. 1999a, *ApJ*, 524, L19

Moore, B., Quinn, T., Governato, F., Stadel, J., & Lake, G. 1999b, *MNRAS*, 310, 1147

Sand, D. J., Treu, T., & Ellis, R. S. 2002, *ApJ*, 574, L129

Spergel, D. N., & Steinhardt, P. J. 2000, *Phys. Rev. Lett.*, 84, 3760

Springel, V., & Farrar, G. 2007 (in press, astro-ph/0703232)

Springel, V. 2005, *MNRAS*, 364, 1105

Yoshida, N., Springel, V., White, S. D. M., Tormen, G. 2000a, 535, L103

Yoshida, N., Springel, V., White, S. D. M., Tormen, G. 2000b, 544, L87

Table 1. Initial Simulation Parameters

Run Name	$N_{DM}$	$\sigma/m$ ( $\text{cm}^2 \text{ g}^{-1}$ )	$\rho_{c,1}$ ( $10^6 \text{ M}_\odot \text{ kpc}^{-3}$ )	$r_{c,1}$ (kpc)	$\rho_{c,2}$ ( $10^6 \text{ M}_\odot \text{ kpc}^{-3}$ )	$r_{c,2}$ (kpc)
R1	$10^6$	0	3.27	213	4.59	149
R2	$10^6$	0.24	3.27	213	4.59	149
R3	$10^6$	0.48	4.42	183	6.57	129
R4	$10^6$	0.72	7.03	151	11.75	108
R5	$10^6$	0.96	6.26	167	9.76	124
R6	$10^6$	1.25	6.26	167	9.76	124

Table 2. Conditions at Observed Separation

Run Name	$N_{DM}$	$\sigma/m$ ( $\text{cm}^2 \text{ g}^{-1}$ )	$M_1(r < 150\text{kpc})$ ( $10^{13} \text{ M}_\odot$ )	$M_2(r < 150\text{kpc})$ ( $10^{13} \text{ M}_\odot$ )	$\Delta x^a$ (kpc)	$f^b$
R1	$10^6$	0	12.0	11.1	1.8	0.0
R2	$10^6$	0.24	11.5	10.4	5.4	0.08
R3	$10^6$	0.48	11.8	10.4	15.0	0.16
R4	$10^6$	0.72	12.6	11.0	24.1	0.27
R5	$10^6$	0.96	12.4	10.9	37.9	0.32
R6	$10^6$	1.25	11.4	9.8	53.9	0.38
Obs.			$11.9 \pm 1.6$	$10.6 \pm 0.4$	$25 \pm 29$	$0.16 \pm 0.07$

<sup>a</sup> $\Delta x$  is the offset between the subcluster total mass and galaxy centroids.

<sup>b</sup> $f$  is the fractional decrease in the mass-to-light ratio of the subcluster within 150 kpc.

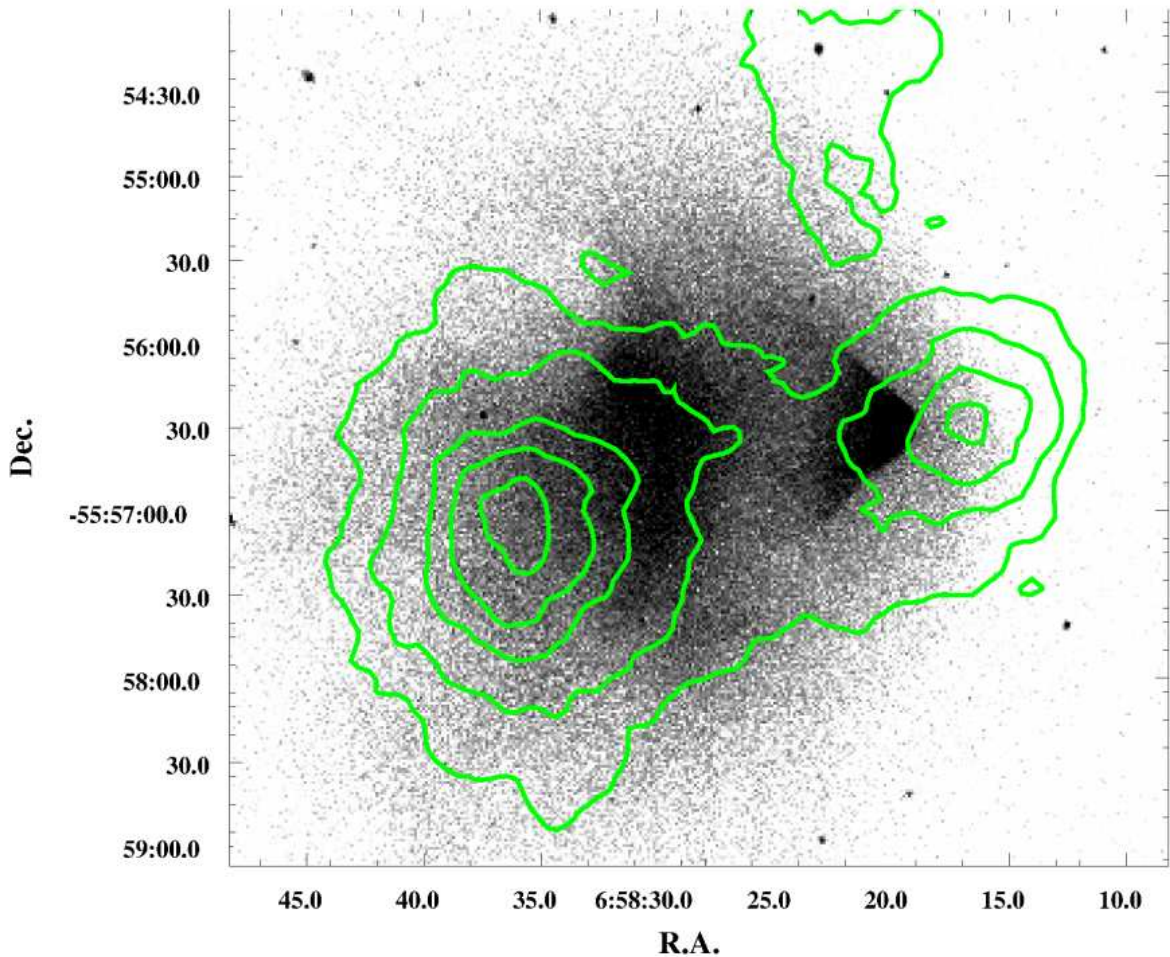


Fig. 1.— X-ray image with weak lensing mass contours overlaid. The gas bullet lags the subcluster DM halo. The current separation of the subcluster and main cluster mass peaks is 720 kpc.

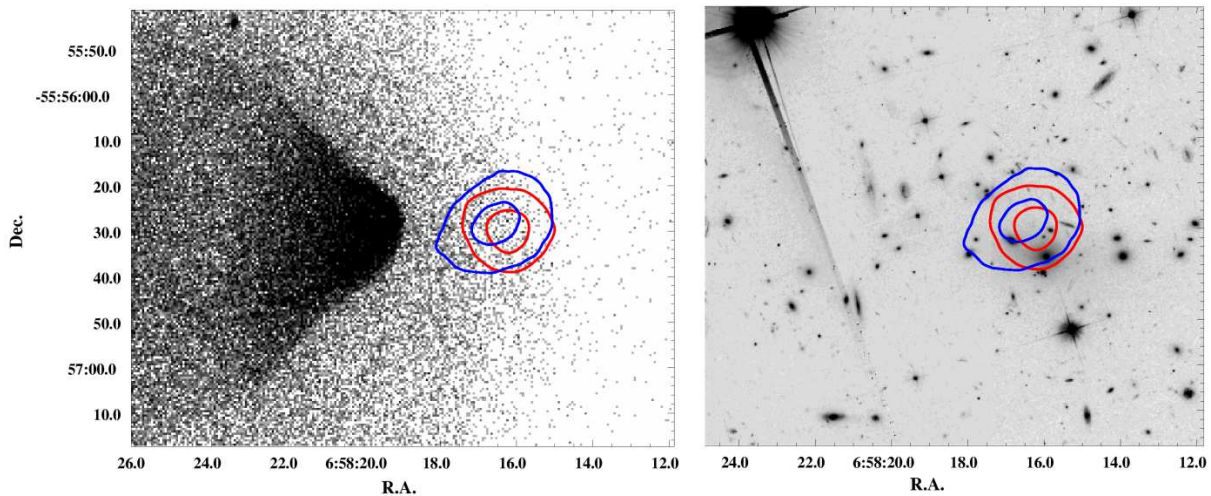


Fig. 2.— Close up of the subcluster bullet region, with the DM (blue) and galaxy (red) centroid error contours overlain. The contours show the 68.3% and 99.7% error regions. The left panel shows the X-ray *Chandra* image, while the right shows the optical *HST* image.

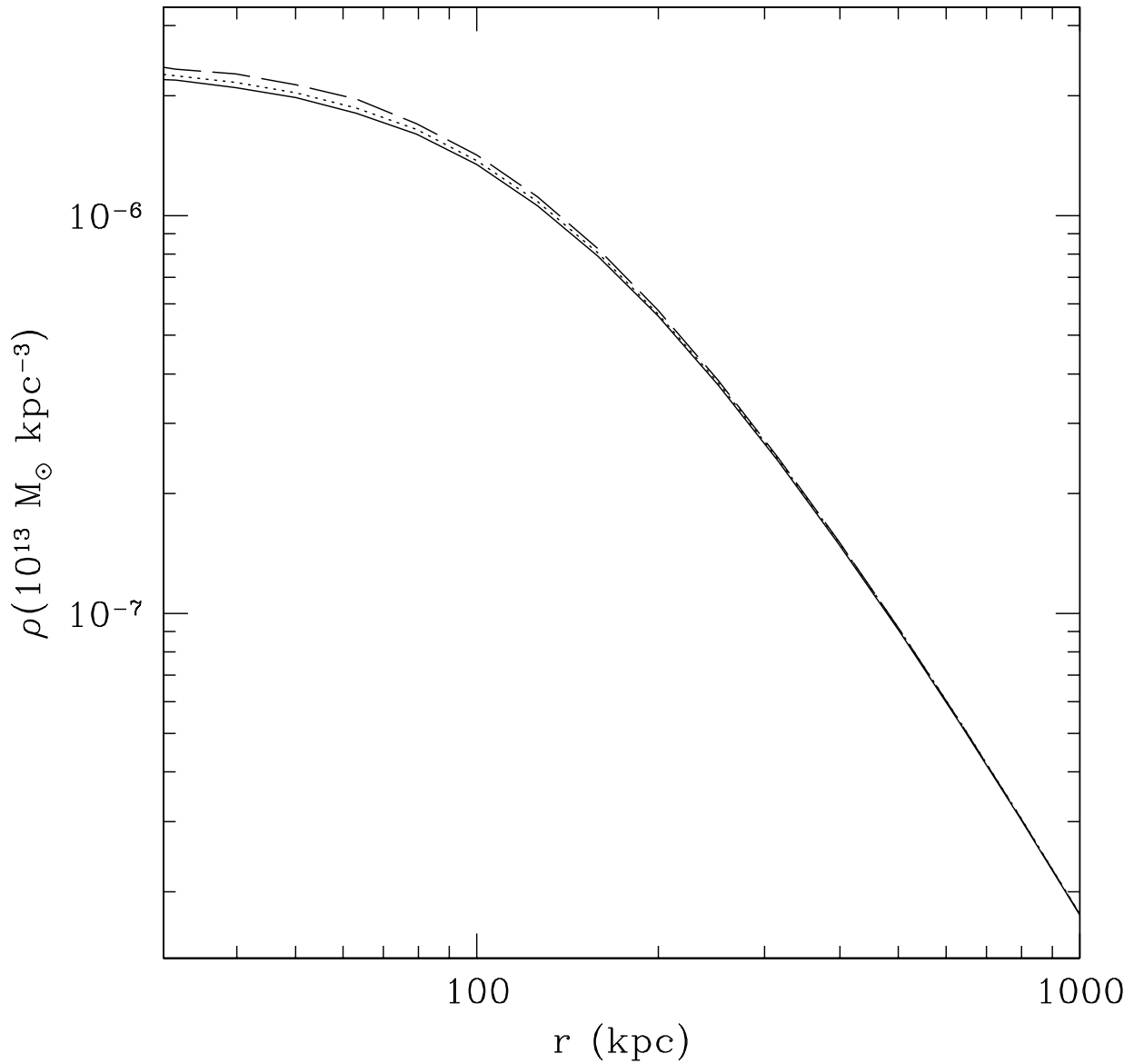


Fig. 3.— Density profile of an isolated King model cluster at  $t = 0$  (solid line), and after evolving for 1 Gyr with  $\sigma/m = 0$  (dotted line) and  $\sigma/m = 0.7 \text{ cm}^2 \text{ g}^{-1}$  (dashed line).

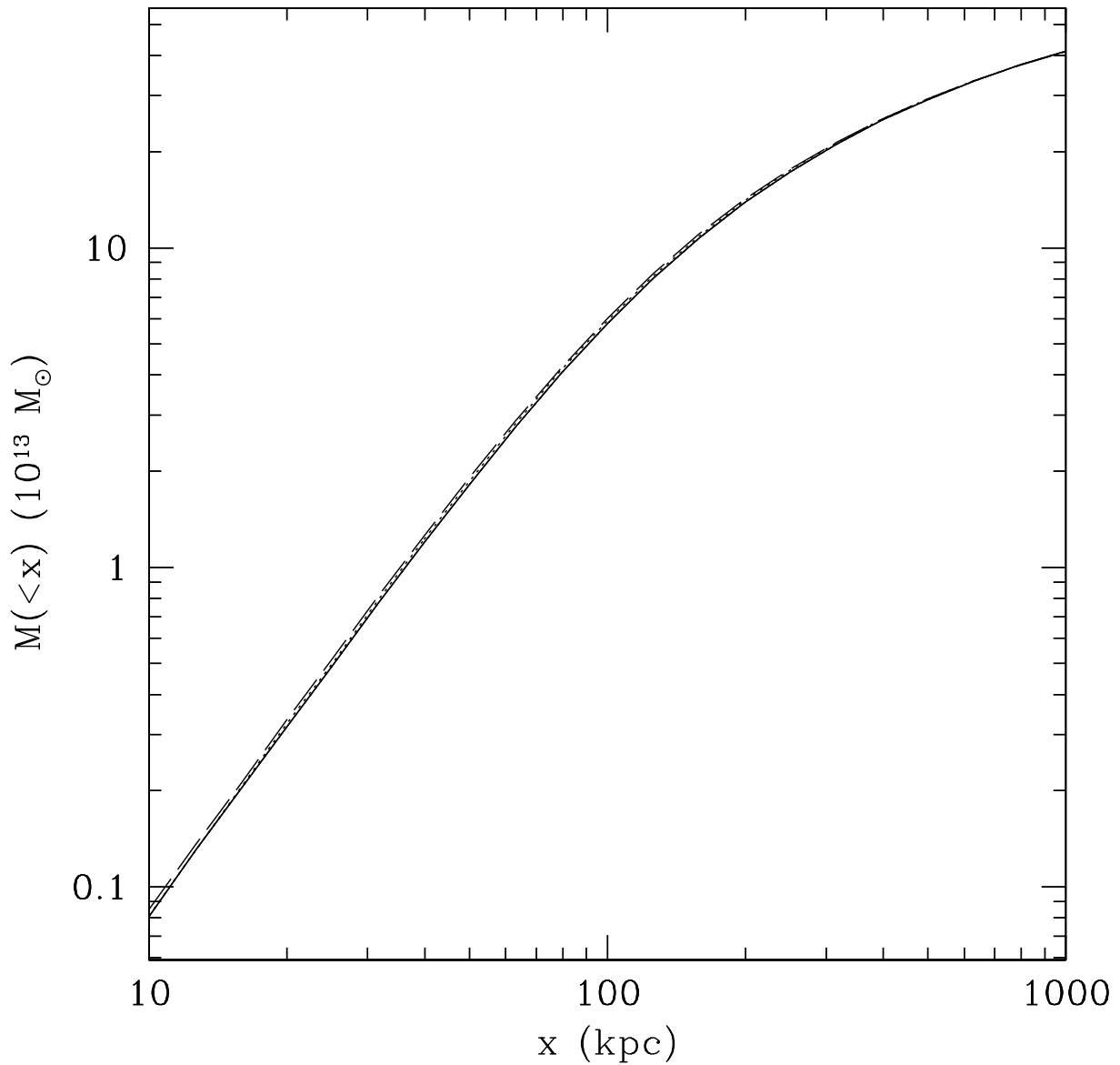


Fig. 4.— Total mass within projected radius  $x$  for the cluster plotted in Figure 3. Line-type indications are the same as in Figure 3.

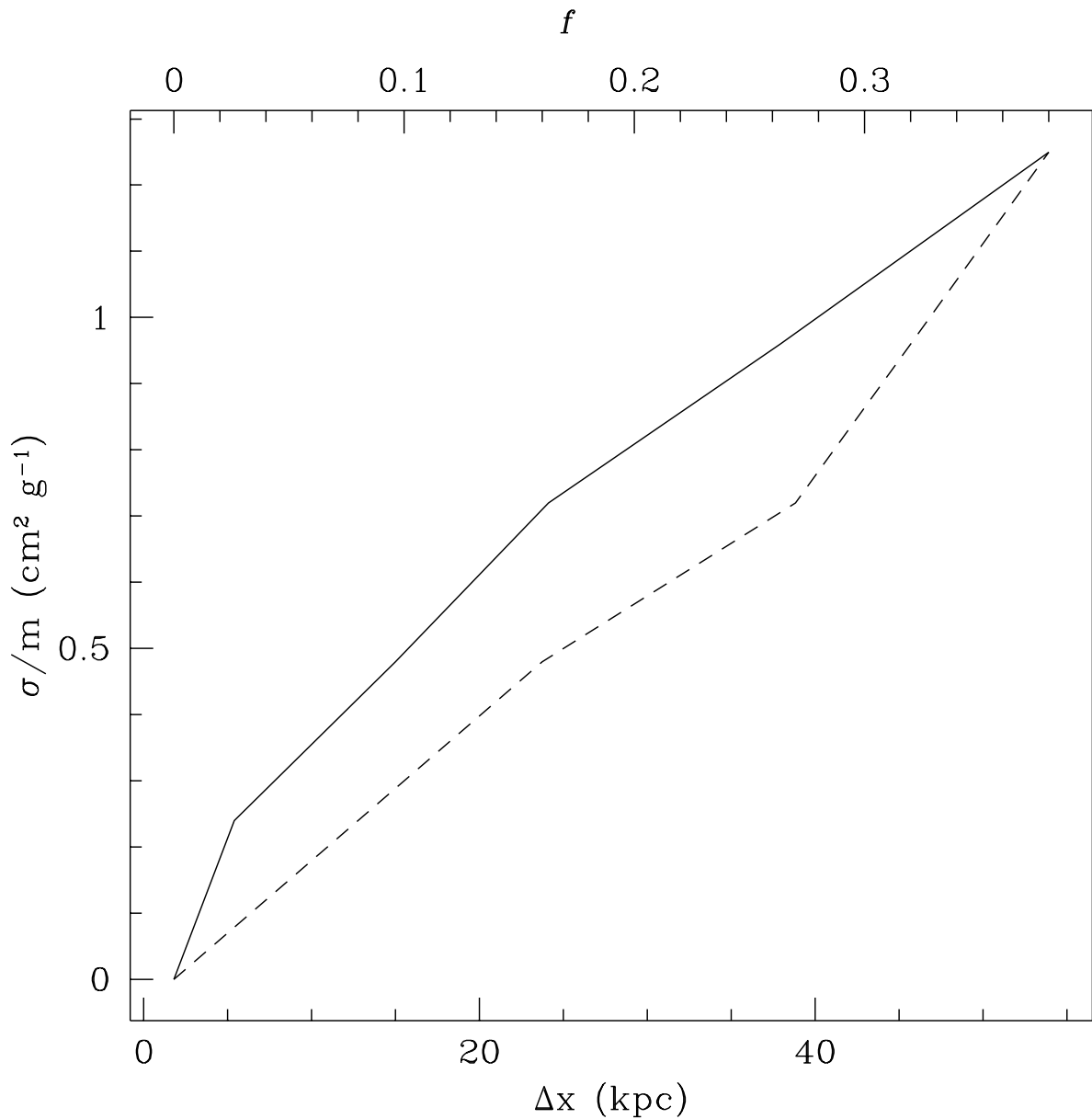


Fig. 5.— The dependence of the subcluster galaxy and total mass centroid offset ( $\Delta x$ , solid line) and the fractional change in the subcluster  $M/L$  ratio ( $f$ , dashed line) on  $\sigma/m$ . Based on the values given in Table 2.